Dalton Transactions

Accepted Manuscript

ROYAL SOCIETY OF CHEMISTRY

www.rsc.org/dalton

Fabrication of $CoTiO_3$-TiO_2 Composite Films from Heterobimetallic Single Source Precursor for Electrochemical Sensing of Dopamine

Muhammad Ali Ehsan,[a] Rabia Naeem,[b] Hamid Khaledi,[c] Manzar Sohail,[a] Abbas Hakeem Saeed,[a] Muhammad Mazhar [b]*

[*a*] Center of Research Excellence in Nanotechnology (CENT), King Fahd University of Petrolium & Minerals, Saudia Arabia.

[*b*]*Department of Chemistry, Faculty of Science, University of Malaya, Lembah Pantai, 50603-Kuala Lumpur, Malaysia.

[*c*] Department of Chemistry, University of the Pacific, 3601 Pacific Avenue, Stockton, CA 95211, USA

**Corresponding author's e-mail*: mazhar42pk@yahoo.com, Tel.: +60379674269;

Fax: +60379674193

Abstract

Cobalt titanate-titania composite oxide films have been grown on FTO- coated glass substrates from a single-source heterometallic complex $[Co_2Ti_4(\mu\text{-}O)_6(TFA)_8(THF)_6]\cdot THF$ (**1**) which was obtained in quantitative yield from the reaction of diacetatocobalt(II) tetrahydrate, tetraisopropoxytitanium(IV), and trifluoroacetic acid from a tetrahydrofuran solution. Physicochemical investigations of complex (**1**) has been carried out by melting point, FT-IR, thermogravimetric and single-crystal X-ray diffraction analysis. $CoTiO_3$-TiO_2 films having spherical objects of various sizes have been grown from (**1**) by aerosol-assisted chemical vapor deposition at different temperatures of 500, 550 and 600 °C. Thin films characterized by XRD, Raman and X-ray photoelectron spectroscopies, scanning electron microscopy, energy-dispersive X-ray analysis have been explored for electrochemical detection of dopamine (DA). The cyclic

volatammetry with the $CoTiO_3$-TiO_2 electrode showed DA oxidation peak at + 0.215 V while linear sweep voltammetry displayed a detection limit (LoD) of 0.083 μM and a linear concentration range of 20-300 μM for DA. Thus, $CoTiO_3$-TiO_2 electrode is a potential candidate for the sensitive and selective detection of DA.

1. Introduction

Metal titanate-titania ($MTiO_3$-TiO_2) composite materials are becoming increasingly important because of their potential for catalytic[1] and photocatalytic oxidation of organic molecules[2] and water[3] and application as anode materials for Li-ion batteries[4]. Such materials are at the centre of attention because they possess functional properties of both the pure $MTiO_3$ and TiO_2. Hence, such composite materials might perform better in energy and environmental sector than the individual components used alone. For example, the photocatalytic efficiency of $ZnTiO_3$-TiO_2 nanocomposite towards the degradation of methyl orange and pentachlorophenol molecules was compared with pure TiO_2 and results showed that $ZnTiO_3$-TiO_2 composite performed better than pure TiO_2.[5] In a different study, optically transparent $ZnTiO_3$-TiO_2 nanocomposite coatings have also shown remarkable activity in the photomineralization process of fatty-acids.[6] A nanocomposite of $BaTiO_3$-TiO_2 exhibits an increased antibacterial photocatalytic activity under visible light which cannot be attained by using either pure $BaTiO_3$ or TiO_2.[7]

Cobalt titanate ($CoTiO_3$), a member of functional metal titanate family is a well-researched material for gas sensing[8,9] and catalytic[10] applications. But the design and synthesis of distinct $CoTiO_3$-TiO_2 composite system was relatively less explored in the past.[11] Recently, Huo et. al. reported a general route for the synthesis of $MTiO_3$-TiO_2 (M = Zn, Co, Ni) via hydrothermal method.[12] In a different study, attempts to produce

$CoTiO_3$-TiO_2 resulted in the formation of Co_3O_4/TiO_2 heterojunction and the material was investigated for gas sensing applications.[13]

The synthesis of device grade multi-phase oxide thin films with exact stoichiometric and controlled homogeneity at lower temperature is a challenging task and usually two or more separate precursors are used to react under CVD conditions. This procedure, however, makes it difficult to control film stoichiometry and usually high deposition temperatures are required. A viable alternative approach to such materials is to use a heterobimetallic single-source precursor (SSP), which consists of the elements in the material bonded at the core of the molecule, with various other ligands attached to each of the elements.[14,15] The reaction pathway involves adsorption of the precursor without breaking the M–O bond but with loss of the ancillary ligands, affording a thin film of the desired material.[15] The advantages of the SSP approach are fourfold. Firstly, the elemental stoichiometry of the precursor can be retained in the film.[15] Secondly, the high deposition temperatures often associated with multi-source depositions are generally lowered.[15] Thirdly, the precursor delivery system can be simplified[15] and finally a better homogeneity is possible since the desired elements are effectively premixed at the molecular level.[15] Consequently, SSPs can provide a simple and clean route to films, eliminating the need for a mixture of precursors which can often be toxic and/or expensive, as well as involving complicated gas-phase reaction dynamics which can result in the formation of non-stoichiometric films.[15] The consumption of these SSPs in an aerosol assisted chemical vapor deposition (AACVD) has become a well-established route for the design and synthesis of advanced material films. AACVD is a solution-based process, which relies on the solubility of the precursor.[16,17] The process is scalable, allows for the formation of multicomponent materials and the simplification of the precursor delivery stage potentially reduces the cost of the

deposition process.[18] Recently, we reported several well-defined heterobimetallic compounds including $[Cd_2Ti_4(\mu\text{-}O)_6(TFA)_8(THF)_6]$ •1.5THF,[19] $[Zn_2Ti_4(\mu\text{-}O)_6(TFA)_8(THF)_6]$•THF,[20] $[Cu_4Zr_2(\mu_4\text{-}O)_2(dmae)_4(OAc)_8]$•$2H_2O$[21] and $[Cu_4Zr_6(\mu\text{-}O)_8(dmap)_4(OAc)_{12}]$•$H_2O$[22] for the synthesis of composite oxide thin films of $CdTiO_3$-TiO_2, $ZnTiO_3$-TiO_2, $CuZrO_3$-CuO and CuO-$1.5ZrO_2$ respectively, via AACVD method and their possible technological applications were explored. For example, the scope of $CdTiO_3$-TiO_2 composite thin film having band gap of 3.1 eV was investigated as photoanode for dye-sensitized solar cell applications.[19] The $ZnTiO_3$-TiO_2 films grown into a variety of spherical designs at 550 ˚C using three different solvents such as methanol, tetrahydrofuran and acetonitrile were tested for their electrochemical sensing capability towards nitrite ions.[20] Furthur, CuO-$1.5ZrO_2$ composite films developed at 550 ˚C from methanol and ethanol solvents were found promising for electrocatalytic oxidation of methanol that indicated their potential for direct methanol fuel cell application.[22] In contrast to our previous work, we expanded our studies towards biological applications and hence prepared 1:1 $CoTiO_3$: TiO_2 composite thin films by thermolysis of appropriate Co-Ti heterometallic assembly on the substrate surface and the resultant films were explored for dopamine sensing.

The previously known heterobimetallic oxo complexes of Co-Ti metals are not significantly large in numbers and includes $[Co_2Ti(\mu_3\text{-}O)(TFA)_6(THF)_3]$[23] and $[Co(H_2O)_5]_2[Ti(O_2)_2O(nta)_2]\cdot 7H_2O$.[24] Earlier, we utilized the former compound as SSP for deposition of $CoTiO_3$-CoO composite oxide thin films; however the thermolysis of the later yielded $CoTiO_3$ at 700 ˚C. Hexaaquacobalt titanium citrate $(NH_4)_2[Co(H_2O)_6][Ti(H_2cit)_3]_2 \cdot 6H_2O$ has been recognized as a class of molecular precursor compound for the single step synthesis of $CoTiO_3$-TiO_2 nanocomposite powder at 600 ˚C.[25]

Some well-characterized heterobimetallic SSPs $[Sr(H_2O)]_7[Ti(O_2)(edta)]\cdot H_2O$[26], $[Ca(H_2O)_3]_2[Ti_2(O_2)_2O(NC_6H_6O_6)_2]\cdot 2H_2O$[27] and $[ZnMn_2(Hcit)_2\cdot 8H_2O$[28] (where edta = ethylenediaminetetraacetic acid ; $NC_6H_6O_6$ = nitrilotriacetato and Hcit = citric acid) have been reported for the target synthesis of single phase $CaTiO_3$, $SrTiO_3$ and $ZnMn_2O_4$ powders respectively, however these molecular precursors were not utilized in AACVD for thin film deposition. The choice of preparation of single phase or multi-phase oxide via heterobimetallic SSP mainly depends upon the design and synthesis of heterometallic precursor with a certain metallic stoichiometry. The elemental composition of the resultant SSP compound can be tuned by changing the molar ratios of the reactant spices so that they can produce single phase or multiphase oxide materials. For example, a 1:1 (Co: Ti) complex $[Co(H_2O)_5]_2[Ti(O_2)_2O(nta)_2]\cdot 7H_2O$[24] obtained by reacting $CoCl_2\cdot 6H_2O$ with $Ti(OC_4H_9)_4$ in 1:1 stoichiometry produces single phase $CoTiO_3$, while a 1:2 (Co: Ti) compound $(NH_4)_2[Co(H_2O)_6][Ti(H_2cit)_3]_2 \cdot 6H_2O$[25] prepared by the interaction of $CoCl_2\cdot 6H_2O$ with $Ti(OC_4H_9)_4$ in 1: 2 molar ratio generates biphasic $CoTiO_3$-TiO_2 composite on pyrolysis. Similarly, two compounds with different Cd/Ti ratios, $[Cd_4Ti_4(dmae)_4(TFA)_8(OAc)_4O_6]$[29] and $[Cd_2Ti_4(\mu\text{-}O)_6(TFA)_8(THF)_6]\cdot 1.5THF$[19] were designed by different synthetic methods to generate single phase $CdTiO_3$ and multi-phase $CdTiO_3$ -TiO_2 composite respectively.

The protraction of previous synthetic strategy[23] enables us to develop a new heterobimetallic assembly $[Co_2Ti_4(\mu\text{-}O)_6(TFA)_8(THF)_6]\cdot$ THF (**1**) by reacting cobalt (II) acetate with titanium (IV) isopropoxide in a 1: 2 stoichiometry in presence of triflouroacetic acid in THF. The resultant complex exhibits different physicochemical properties from the previously reported $[Co_2Ti(\mu_3\text{-}O)(TFA)_6(THF)_3]$[23] complex and hence the single molecular potential of this complex generates a 1:1 $CoTiO_3$:TiO_2 composite oxide material. Thin films from complex (**1**) were grown

on fluorinated tin oxide (FTO) conducting glass substrate in the temperature range of 500-600 ˚C in air atmosphere. The deposited films were examined by XRD, SEM, EDX and XPS for their phase, structural, textural and compositional recognition and further films were tested for their suitability for electrochemical determination of Dopamine (DA).

Dopamine (DA) is a well-known neurotransmitter which belongs to catecholamine family of neurotransmittors. DA is one of the most abundant neurotransmitter in the body fluids and plays a crucial role in controlling many physiological processes such as learning, memory and motivated behaviors. DA deficiency in the body can cause severe neurological disorders and diseases such as Parkinson's and Schizopherine diseases. Furthermore, use of drugs also directly affects the physiological pathways of DA release and transmission in the human body.[30,31] Thus, being such an important neurotransmitter with wide range of implications, attempts for precise electrochemical determination of DA has attracted much attention in the recent research. One approach for the advancement of a DA sensor is to synthesize new materials which can catalyze DA oxidation.

2. Experimental

2.1 Material and methods

All reagents were purchased from Sigma-Aldrich and synthetic work was carried out under an inert atmosphere of dry argon using Schlenk tube fitted with vacuum line and hot plate arrangements. The tetrahydrofuran was rigorously dried over sodium benzophenoate and distilled immediately before use. The melting point was determined in a capillary tube using an electrothermal melting point apparatus; model MP.D Mitamura Riken Kogyo (Japan). Fourier transform infra-red (FT-IR) spectrum was recorded on a single reflectance ATR instrument (4000–400 cm^{-1}, resolution 4 cm^{-1}). The controlled

thermal analysis was investigated using a Perkin Elmer TGA 4000 thermogravimetric analyzer with a computer interface. The thermal measurements were carried out in a ceramic crucible under an atmosphere of flowing nitrogen (50 mL min^{-1}) with a heating rate of 10 °C min^{-1}.

2.2 Synthesis of $[Co_2Ti_4(\mu\text{-}O)_6(TFA)_8(THF)_6]\cdot THF$ (1)

Complex (**1**) was prepared by mixing stoichiometric amounts of 0.50 g (2.0 mmol) of $Co(CH_3COO)_2\cdot(H_2O)_4$ and 1.19 mL (4.0 mmol) of $Ti(OCH(CH_3)_2)_4$ followed by the addition of 1.21 mL (16.0 mmol) of CF_3COOH in 25 mL of THF in a 50mL Schlenk tube. The reaction mixture was stirred for 4h and solvent was evacuated under vacuum to obtain a red powder which was re-dissolved in THF. The resulting transparent solution was cannula-filtered and placed at room temperature for 2 days to obtain the red block shape crystals of complex (**1**) in 75% yield.

Mp: 195 °C (decomposition). IR: ν_{max}/cm^{-1} 2989w, 2904w, 1717s, 1681s, 1469s, 1388w, 1329w, 1198s, 1148s, 1025w, 1038w, 899w, 792s, 722s, 681w, 654w, 618s, 585w, 493s, 474s. TGA: 50-95 °C (1.53% wt. loss); 100-180 °C (7.2% wt. loss); 181-225 °C (23.6% wt. loss), 250-500 °C (40.17% wt. loss) (Residual mass of 27.50%); (Cal. for $CoTiO_3$-TiO_2 25.80%).

2.3. Single-crystal X-ray crystallography

Diffraction data for the crystal were collected on an Agilent SuperNova Dual diffractometer with an Atlas detector (graphite-monochromatized Mo-*K*α radiation, λ = 0.71073 Å) at 100(2) K. The data were processed using CrysAlisPro, Agilent Technologies, Version 1.171.37.34 (release 22-05-2014 CrysAlis171.NET) and empirical absorption correction using spherical harmonics implemented in SCALE3 ABSPACK scaling algorithm. The structure was solved using the

program SHELXT and was refined by the full matrix least-squares method on F^2 with SHELXL-2014/7.[32] All the non-hydrogen atoms were refined anisotropically. All the hydrogen atoms were placed at calculated positions and were treated as riding on their parent atoms. The structure exhibits a whole molecule disorder with the two components being related by a pseudo-inversion center. The occupancy of the main component refined to 0.640(2). The structure was also refined as a racemic twin with the twin parameter of 0.46(4). Drawing of the molecule was produced with *Mercury*.[33] Crystal data: $C_{44}H_{56}Co_2F_{24}O_{29}Ti_4$, M_r = 1814.34, pink block, 0.49 × 0.28 × 0.26 mm^3, orthorhombic, *Pca*2$_1$, a = 19.2672(4), b = 20.5759(5), c = 17.2453(4) Å, V = 6836.7(3) Å^3, Z = 4, D_c = 1.763 Mg/m^3, 135126 measured reflections, 19480 unique reflections (R_{int} = 0.0517), 14499 observed reflections [(I > 2σ(I)], final R indices [(I > 2σ(I)]: R_1 = 0.0858, wR_2 = 0.2091. CCDC No. 1453304.

2.4. Deposition of thin films by AACVD

An in-house designed AACVD set up was used for the growth of $CoTiO_3$-TiO_2 oxide composite on commercially available FTO conducting glass substrates. The substrates were cleaned with detergent, distilled water, acetone and ethyl alcohol, to remove surface grease then placed inside the reactor tube and furnace (CARBOLITE, Model No. 10/25/130) (6"L × 1"D) and heated up to the desired deposition temperature for 10 minutes. Thin film deposition experiments were performed at three different temperatures of 500, 550 and 600 ˚C, respectively from 20 mL of 0.1M solutions of precursor (**1)** in ethanol. In a typical deposition experiment, a precursor solution was taken in a 50mL round bottom flask which was immersed in water bath above the piezoelectric modulator of an ultrasonic humidifier (Model No. Cool Mist-plus serial No. ADV-CMP-85956). Air at a flow rate of 100 mL min^{-1} was used as the carrier gas and the flow rate was controlled by an L1X linear flow meter. The generated aerosol droplets were then

transferred into the hot wall zone of the reactor by the carrier gas. Both the solvent and precursor were evaporated and the precursor vapour reached the heated substrate surface where thermally induced reactions and subsequent film deposition took place.

2.5. Thin film analysis

X-ray diffraction (XRD) measurements were obtained using a PANanalytical, X'Pert HighScore diffractometer with primary monochromatic high intensity CuK_α (λ = 1.5418 Å) radiation over Bragg angles ranging from 10 to 90° in a step size of 0.026° while the operating voltage and current were maintained at 30kV and 40mA respectively. Raman spectroscopic measurements were carried out on a Renishaw InVia Raman microscope and excitation was performed using the 514 nm line of Argon laser with a 0.01 mW output power. Scanning electron microscopy (Hitachi FESEM SU 8000) equipped with an energy dispersive X-ray spectrometer EDX (INCA Energy 200, Oxford Inst.) was used to determine the films morphology and elemental stchiometry. X-ray photoelectron spectroscopy (XPS) analysis of the films was carried out using an ULVAC-PHI Quantera II with a 32-channel Spherical Capacitor Energy Analyzer under vacuum (1 x 10^{-6} Pa) using Monochromated Al Kα radiation (1486.8eV) and natural energy width of 680meV. The carbonaceous C 1s line (284.6 eV) was used as a reference to calibrate the binding energies.

2.6. Electrochemical studies for dopamine sensing

All the electrochemical experiments were performed in a single compartment three–electrode cell at room temperature using a PAR-VersaSTAT-3 Electrochemical workstation. The $CoTiO_3$-TiO_2 composite film and a platinum wire were used as working and counter electrodes, respectively. Silver/silver chloride (Ag/AgCl) electrode was used as a reference electrode. All studies for DA were carried out at pH 7.0 using a phosphate buffer solution. All solutions for

electrochemical experiments were prepared with Millipore water having a resistivity of 18.2 M (Purelab Classic Corp., USA).

3. Results and discussion

3.1. Synthesis and characterization of complex (1)

The design and synthesis of heterobimetallic complex $[Co_2Ti_4(\mu\text{-}O)_6(TFA)_8(THF)_6]\cdot THF$ (**1**) ensues through chemical interaction of diacetatocobalt(II) with tetrakisisopropoxytitanium(IV) upon addition of a trifluoroacetic acid as a bridging moiety in THF. The current workup gave complex (**1**) in 75 % yield in form of red crystals and is stable to air and moisture and soluble in common organic solvent such as methanol, ethanol, THF and acetonitrile.

The composition and stoichiometry of complex (**1**) is established by single crystal X-ray analysis and the presence of bridging functional groups between Co-Ti atoms was also ascertained by FT-IR spectroscopy. The characteristics symmetric and asymmetric ν(C=O) vibrations of trifluoroacetato ligand appear at 1681s and 1469s cm^{-1} respectively. The difference of $\Delta = 212$ cm^{-1} between the symmetric and asymmetric stretching vibrations is attributed to the bidentate bridging carboxylato group of trifluoroacetato ligand that is bonded to different metal centers of the acetate group.[18,20] Similarly, the peak at 1197 cm^{-1} confirms the presence of C–F bonds in complex (**1**).

3.2 Molecular Structure of $[Co_2Ti_4(\mu\text{-}O)_6(TFA)_8(THF)_6]\cdot THF$ (1)

The molecular structure of the Co-Ti complex is depicted in Fig. 1 and a schematic drawing for the molecule is given in Fig. 2.

The structure of the Co-Ti complex resembles those of the analogous Fe-Ti,[18] Cd-Ti,[19] and Zn-Ti[20] complexes, being isostructural with the latter two complexes. The molecule has a non-crystallographic D_2 point symmetry and consists of a Ti_4O_6 core arranged in an adamantane-like

structure. Two of the core O atoms (O1, O6) are of the μ_3-type that bridge pairs of the tetrahedrally located Ti's to the two Co^{II} centers. The other four O atoms (O2, O3, O4, O5) link only pairs of the Ti atoms. Each metal center in the structure is in an octahedral coordination environment made of six O atoms from the Ti_4O_6 cage, TFA's and THF ligands. Table 1 lists the coordination bond lengths for the structure. The Ti-Ti separations are between 3.328-3.352 Å which are comparable to those in the analogous structures.

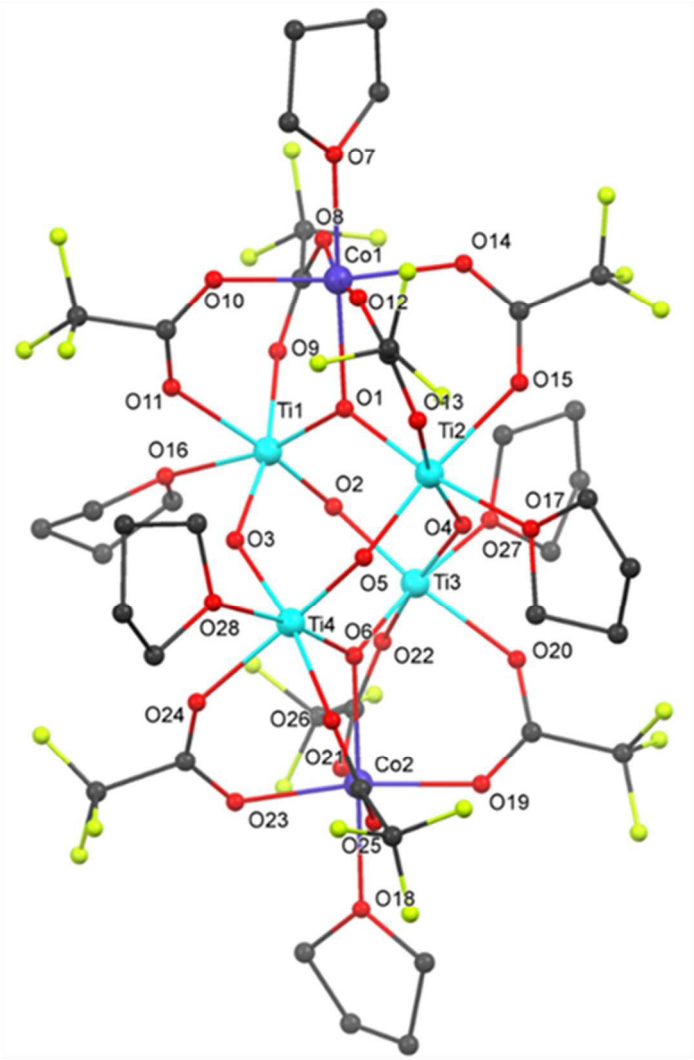

Figure 1: Crystal structure of complex $[Co_2Ti_4(\mu\text{-}O)_6(TFA)_8(THF)_6]\cdot THF$ (**1**). The minor component of disorder, hydrogen atoms, and the solvate THF molecule are not shown.

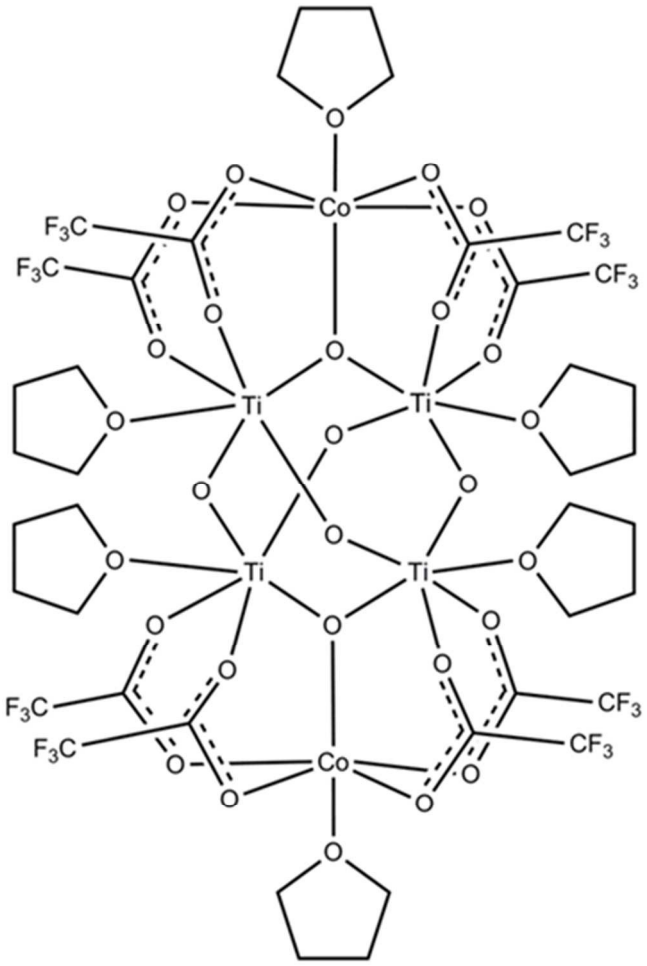

Figure 2: Schematic diagram of complex $[Co_2Ti_4(\mu\text{-}O)_6(TFA)_8(THF)_6]\cdot THF$ (**1**).

Table 1. Coordination bond lengths for $[Co_2Ti_4(\mu\text{-}O)_6(TFA)_8(THF)_6]\cdot$ THF **(1)**

Co(1)-O(1)	2.175(6)	Ti(2)-O(13)	2.080(12)
Co(1)-O(7)	2.111(7)	Ti(2)-O(15)	2.108(10)
Co(1)-O(8)	2.039(8)	Ti(2)-O(17)	2.168(9)
Co(1)-O(10)	2.064(7)	Ti(3)-O(2)	1.860(8)

Co(1)-O(12)	2.083(8)	Ti(3)-O(4)	1.744(8)
Co(1)-O(14)	2.079(8)	Ti(3)-O(6)	1.881(7)
Co(2)-O(6)	2.154(7)	Ti(3)-O(20)	2.079(13)
Co(2)-O(18)	2.108(6)	Ti(3)-O(22)	2.101(12)
Co(2)-O(19)	2.030(11)	Ti(3)-O(27)	2.179(8)
Co(2)-O(21)	2.035(8)	Ti(4)-O(3)	1.851(8)
Co(2)-O(25)	2.041(8)	Ti(4)-O(5)	1.782(8)
Co(2)-O(23)	2.046(8)	Ti(4)-O(6)	1.925(7)
Ti(1)-O(1)	1.853(7)	Ti(4)-O(24)	2.067(9)
Ti(1)-O(2)	1.809(8)	Ti(4)-O(26)	2.116(11)
Ti(1)-O(3)	1.792(8)	Ti(4)-O(28)	2.161(9)
Ti(1)-O(9)	2.092(13)	Ti(1)-Ti(2)	3.347(4)
Ti(1)-O(11)	2.085(10)	Ti(1)-Ti(3)	3.328(4)
Ti(1)-O(16)	2.155(10)	Ti(1)-Ti(4)	3.345(4)
Ti(2)-O(1)	1.938(7)	Ti(2)-Ti(3)	3.347(4)
Ti(2)-O(5)	1.813(8)	Ti(2)-Ti(4)	3.338(4)
Ti(2)-O(4)	1.870(8)	Ti(3)-Ti(4)	3.352(4)

3.3 Thermal analysis of complex (1)

The thermal pyrolysis of complex (**1**) was investigated by thermogravimetric (TG) and derivative thermogravimetric (DTG) analysis in a flowing N_2 atmosphere at the rate of 25 cm^3 min^{-1} and a heating rate of 10 °C min^{-1} and results are displayed in Fig. 3.

The TG (red) and DTG (black) curves in Fig 3 indicate that complete thermal degradation of complex (**1**) occurs in five consecutive weight loss stages of 1.53, 7.2, 16.8, 6.8 and 40.17% which appear at maximum heat intake steps at 72, 160, 195, 218, and 292 ˚C respectively. The weight loss phases are completed at 500 °C yielding steady residues of 27.5 % of its original mass which is equitable with the formation of the expected 1:1 of $CoTiO_3$: TiO_2 (25.80%) composite oxide material from (**1**). Further sintering of the observed residue to the higher temperature of 900 °C did not produce any change in weight,

suggesting that complex (**1**) decomposes quantitatively to endow $CoTiO_3$–TiO_2 as a stable final product.

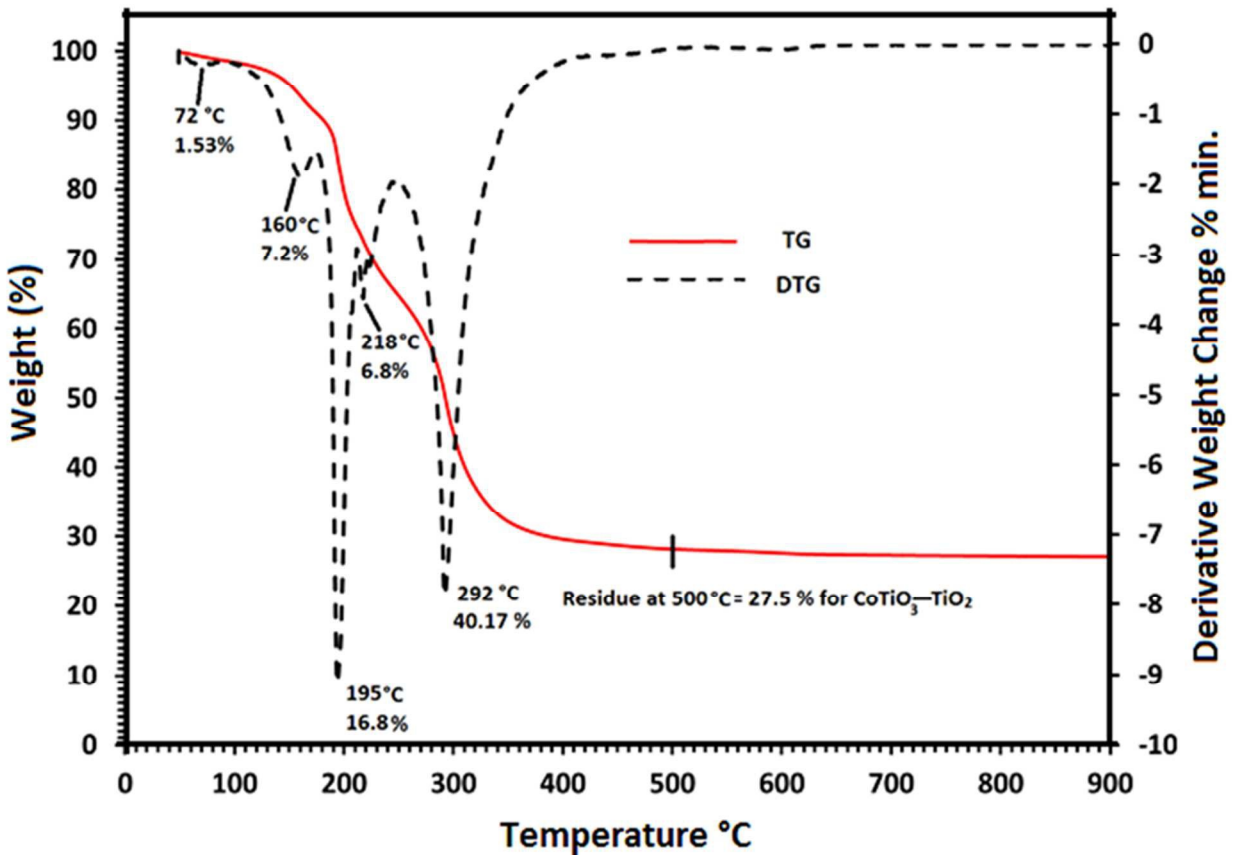

Figure 3: TG (red) and DTG (dotted black) traces of thermal decomposition of complex (**1**) as a function of temperature

3.4 XRD analysis

The ability of complex (**1**) to act as a single source precursor (SSP) for the formation of advanced composite oxides thin film was investigated by AACVD and film deposition experiments were carried out on FTO glass substrate at three different temperatures of 500, 550 and 600 ˚C using ethanolic solution of complex (**1**) in air ambient.

The structural characterization of crystalline deposit was made by XRD analysis and resultant patterns as function of substrate temperature are overlaid in Fig. 4.

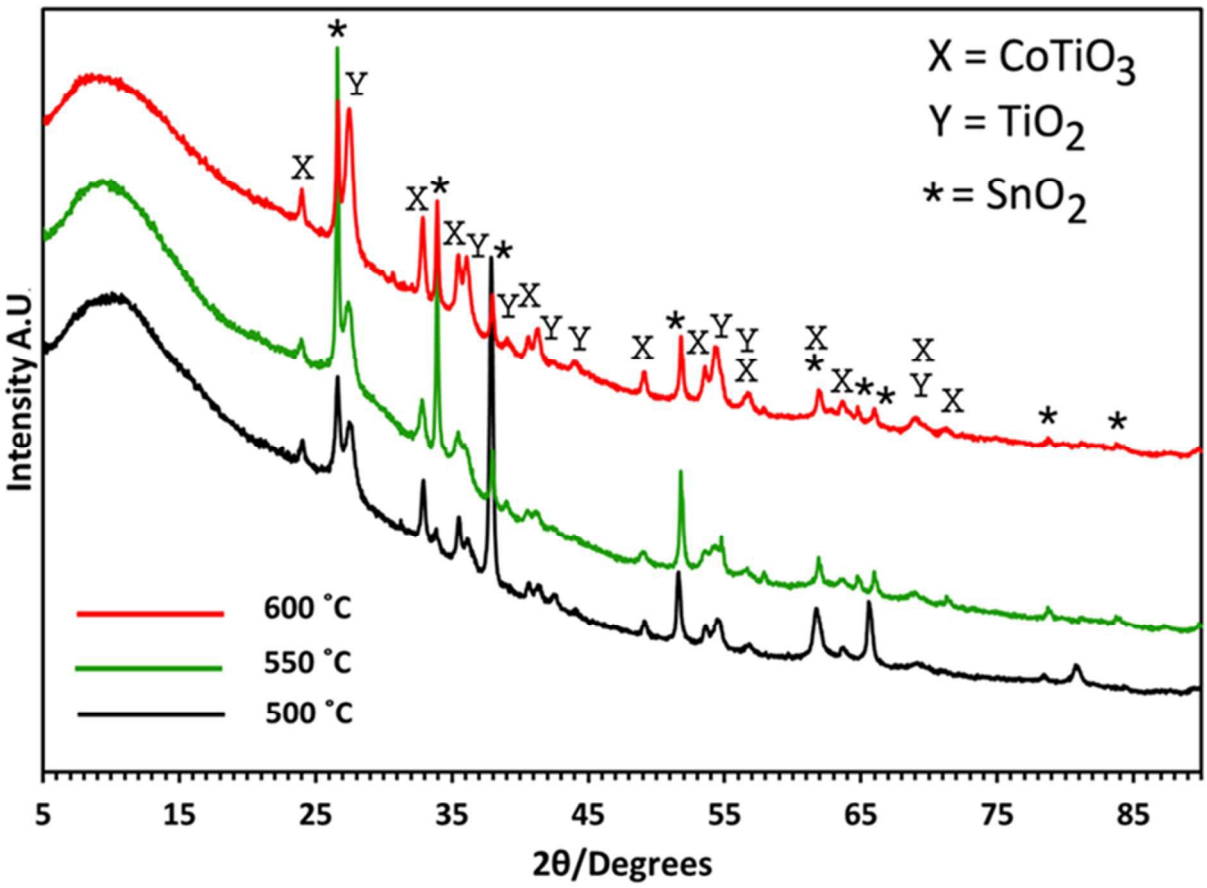

Figure 4: XRD patterns of $CoTiO_3$-TiO_2 composite films deposited on FTO glass substrate at different temperatures of 500 ˚C (black line), 550 ˚C (green line) and 600 ˚C (red line) from ethanolic solution of precursor (**1**). (X) indicates peaks originating from ilmenite-$CoTiO_3$ ((ICSD 98-001-6548)), (Y) specifies peaks related to rutile TiO_2 (ICSD 98-001-6636).

Each XRD pattern in Fig. 4 was analyzed by qualitative phase analysis which indicates the presence of similar cobalt titanium oxide $CoTiO_3$ (ICSD 98-001-6548)[34] and rutile TiO_2 (ICSD 98-001-6636)[35] phases in all the cases. In all films, the prepared $CoTiO_3$ exists in a hexagonal crystal system with space group R-3 and produced characteristic peaks indicated by (**X**) at 2θ = 23.9, 32.8, 35.4, 40.5, 49.0, 53.5, 61.9 and 63.6 ˚ as observed by their Miller indices (012), (104), (2-10), (2-13), (024), (116), (214) and (030), respectively. The emergence of peaks at 2θ = 27.4 (110), 36.0 (011), 41.3 (111), 44.0 (120) and 54.3˚ (121) denoted by (**Y**) are well indexed to

tetragonal rutile TiO_2. The X-ray diffractograms also demonstrate overlapped peaks between $CoTiO_3$ and rutile TiO_2 phases at 2θ values of 56.7, and 68.9˚. Peaks indicated by (*) are originated from crystalline SnO_2 of the FTO substrate. Interestingly, all the XRD patterns show similar phases of ilmenite $CoTiO_3$ and rutile TiO_2 as end product prepared at different temperatures and no sign of phase transformation or growth of impurity phases such as CoO, Co_3O_4 and other titania varieties is perceived from these XRD results.

In comparison with recent literature, the cobalt titanate material is usually prepared at higher temperature of 600 ˚C and prolong heating is often required to improve the crystallinity of the product.[11,36,37] This post sintering process deteriorates the phase purity of the product by generating various unwanted phases and undermines the worth of the material for technological applications.

In comparison well crystallized $CoTiO_3$-TiO_2 composite oxide is formed at lower temperature of 500 ˚C and product remain pure and stable until 600 ˚C which is a unique aspect of using precursor (**1**) in conjugation with AACVD.

3.5 Raman Spectroscopy

The chemical structure and identity of cobalt titanate and titanium dioxide phases in the composite films were further characterized from FT-Raman spectroscopy and the spectra of as-deposited films at different temperatures are comparatively shown in Fig. 5. According to the literature, the Raman scattering modes appeared at 207, 235, 267, 335, 382, 604 and 696 cm^{-1} witness the presence of ilmenite $CoTiO_3$ phase in all cases.[36,10] The most typical feature of $CoTiO_3$ is the strong Raman mode observed near 700 cm^{-1}. This mode arises from the highest frequency vibrational mode of CoO6 octahedra that is the symmetric stretching mode (A_{1g} symmetry for regular Oh octahedral).[36] The characteristic Raman active band for ruitle TiO_2[38,39]

phase is observed at 447 cm^{-1} while the other expected absorptions bands of 246 and 601 seem to merge with the broad peaks of 235 and 604 of $CoTiO_3$. These results indicate formation of phase pure $CoTiO_3$ and rutile TiO_2 in all cobalt titanate-titania composite films prepared at different temperatures of 500, 550 and 600 ˚C.

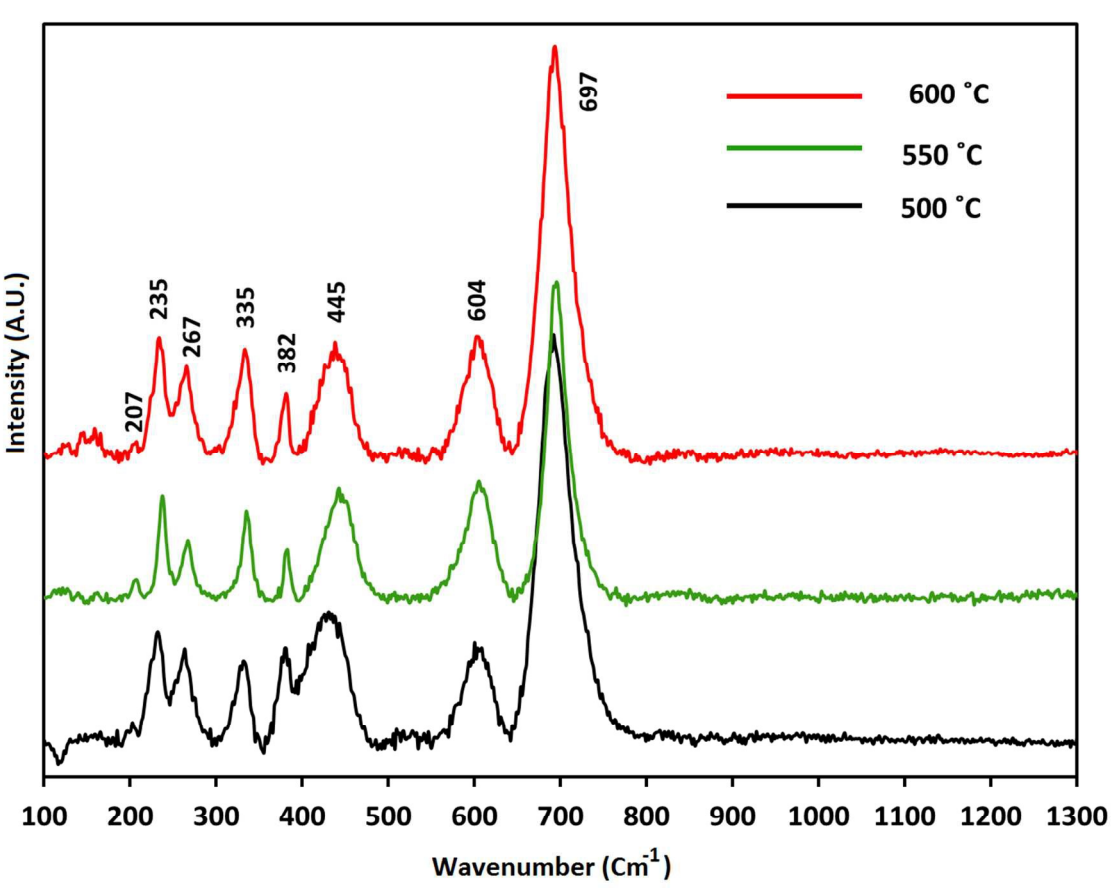

Figure 5: FT-Raman spectra of $CoTiO_3$-TiO_2 composite films deposited at different temperatures of 500 ˚C (black line), 550 ˚C (green line) and 600 ˚C (red line).

3.6 Microstructural properties

The surface morphology, architectures and cross sectional views of $CoTiO_3$-TiO_2 composite films developed at 500, 550 and 600 °C from ethanol solutions of the precursor (**1**) are shown in Fig. 6. Fig. 6a shows that the surface topography of the $CoTiO_3$-TiO_2 film deposited at 500 ˚C is composed of spherical objects of two different types of

microspheres which are grown in horizontal and vertical directions of the substrate surface and are in the size range of 0.3-0.9µm. The surface of one type of microsphere contains buds while others are relatively bare. The cross sectional view of $CoTiO_3$-TiO_2 composite film prepared at 500 ˚C is displayed in Fig. 6(**b**) where small grains developed on the boundary layer of the FTO substrate can be clearly seen and film average thickness was measured to be 4.5 µm.

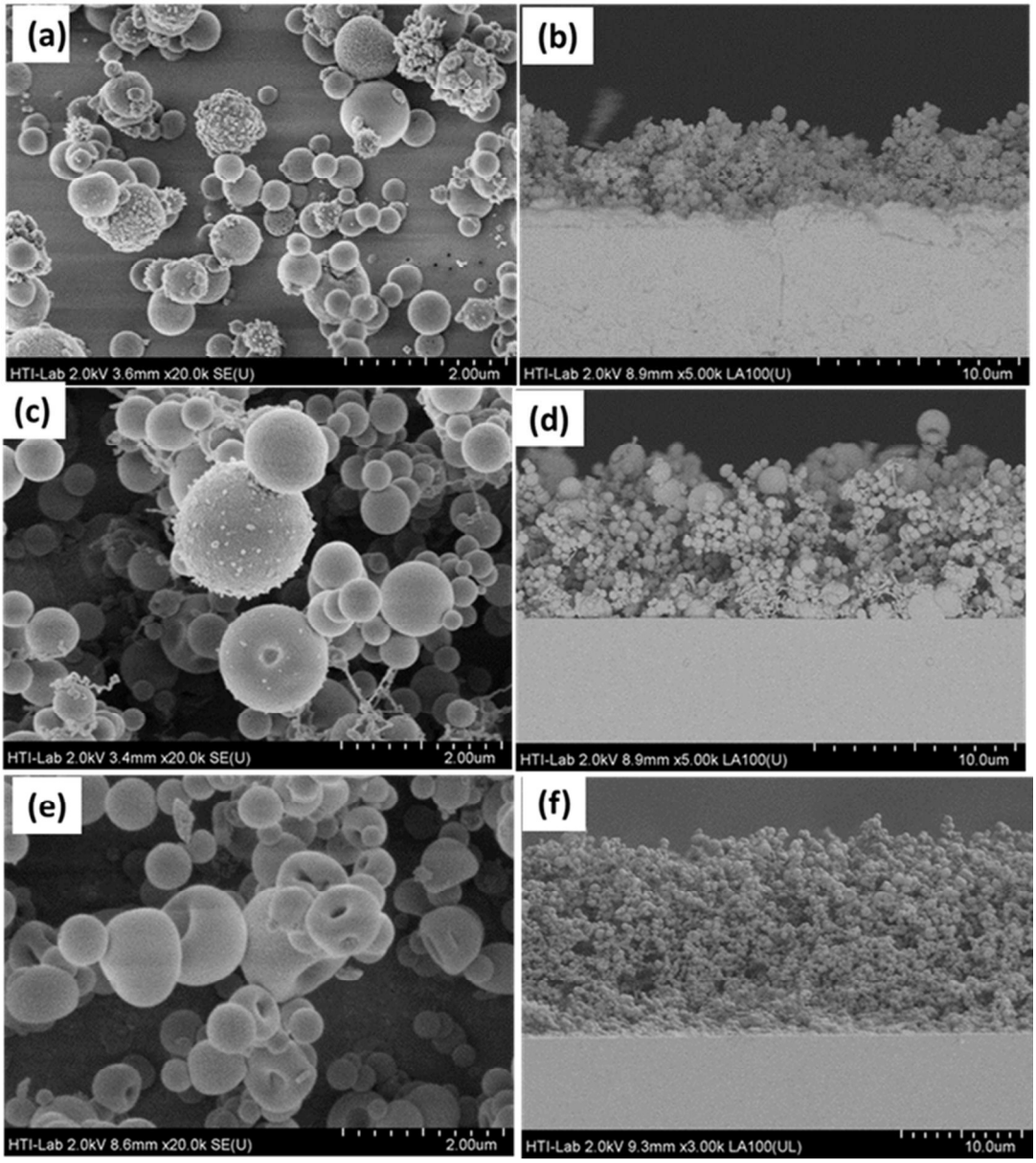

Figure 6: (**a**), (**c**) and (**e**) show surface and (**b**), (**d**) and (**f**) indicate the cross sectional SEM images of $CoTiO_3$-TiO_2 composite thin films deposited on FTO glass substrate from ethanolic solution of precursor (**1**) at temperatures (**a, b**) 500 ˚C (**c, d**) 550 ˚C and (**e, f**) 600 ˚C, respectively.

When the deposition temperature increases to 550 ˚C, the substrate surface is decorated with a new designs of $CoTiO_3$-TiO_2 spherical entities and Fig. 6(**c**) displays that the surface of one kind of spherical object of size 1.12 μm contains tiny particles on its surface while the other type of microsphere of size 0.55 μm exhibits a smooth and plain texture. Fig. 6(**d**) designates the cross sectional view of the $CoTiO_3$-TiO_2 composite film and it is observed that film thickness increases to 7.8 μm with the rise in temperature from 500 to 550 ˚C. Further increasing the deposition temperature to 600 °C results in formation of mixture of donuts and round shaped crystallites of $CoTiO_3$-TiO_2 as displayed in Fig. 6(**e**) and the shape of the thin-film cross sections is shown in Fig. 6(**f**) where a layer of spheroid particles of thickness 18 μm is visibly displayed on the surface of the FTO substrate.

The surface compositions of all films were analysed by energy dispersive analysis (EDX) analysis. EDX spectra shown in SI Fig. 1(**a-c**) were recorded at various arbitrary large areas of the films which revealed that the percent atomic ratio of Co: Ti in the films is almost 1: 2 which is in accordance with the expected 1: 2 elemental ratio present in precursor (**1**). These results confirm that the films grown at different temperatures 500, 550 and 600 ˚C retain the same metallic ratio as found in complex (**1**).

Further the heterogeneity and distribution of cobalt, titanium and oxygen atoms in $CoTiO_3$-TiO_2 composite films was examined by EDX mapping and results are shown in SI Fig. 2 (**a- c**) which

reveal that these atoms are evenly distributed throughout the films matrix confirming the composite nature of all films prepared at different temperatures.

All $CoTiO_3$-TiO_2 films were translucent and light green in colour. The films deposited at lower temperature of 500 and 550 ˚C were robust and adhered strongly on the FTO substrate as verified by the ‘‘Scotch tape test’’ while the film prepared at 600 ˚C showed poor adhesive properties and was failed to qualify the adherence test.

3.7 XPS analysis

The $CoTiO_3$-TiO_2 composite film prepared at 550 ˚C was further examined by X-ray photoelectron spectroscopy (XPS) and results are presented in Fig. 7. The XPS survey scan spectrum in Fig. 7(a) indicates that cobalt, titanium, and oxygen are the major components at the surface of the film. After elements identification, their chemical and valence states were analyzed by narrow scans and results are shown in Fig. 7(b-d).

In the high resolution Ti 2p spectrum , Fig. 7(b), the binding energies of 458.7 and 464.4 eV are indicative of Ti 2p3/2 and Ti 2p1/2 respectively which correspond to Ti^{4+} and matches well with the published data for TiO_2.[36,37] Fig. 7(c), represents O1s spectra where a primary peak at 530 eV can be further divided into sub peaks centered at 529.7 and 530.2 eV attributing to Ti–O , Co–O in $CoTiO_3$, respectively.[36,37] Two peaks at 531.4 and 532.6 eV are assigned to the adsorbed oxygen and hydroxyl oxygen, respectively.

The high resolution Co 2p spectrum is shown in Fig. 7(d). Two main peaks at binding energies of 781.5 and 797.3 eV correspond to Co $2p_{3/2}$ and Co $2p_{1/2}$. The difference (Δ) between Co 2p1/2 and Co 2p3/2 orbital is nearly 16 eV, which implies the fundamental oxidation state of high-spin Co^{2+}, and is very similar to those reported earlier for $CoTiO_3$.[13,10] Moreover, the splitting of the Co 2p1/2–Co 2p3/2 orbital components Δ is usually 15 eV for the low-spin Co^{3+} . Toward the

left of each main peak is a satellite peak known as a shake-up line which occurs when Co (II) resides in a high spin state. Thus, the XPS results strongly suggest the formation of phase pure $CoTiO_3$-TiO_2 composite oxide films.

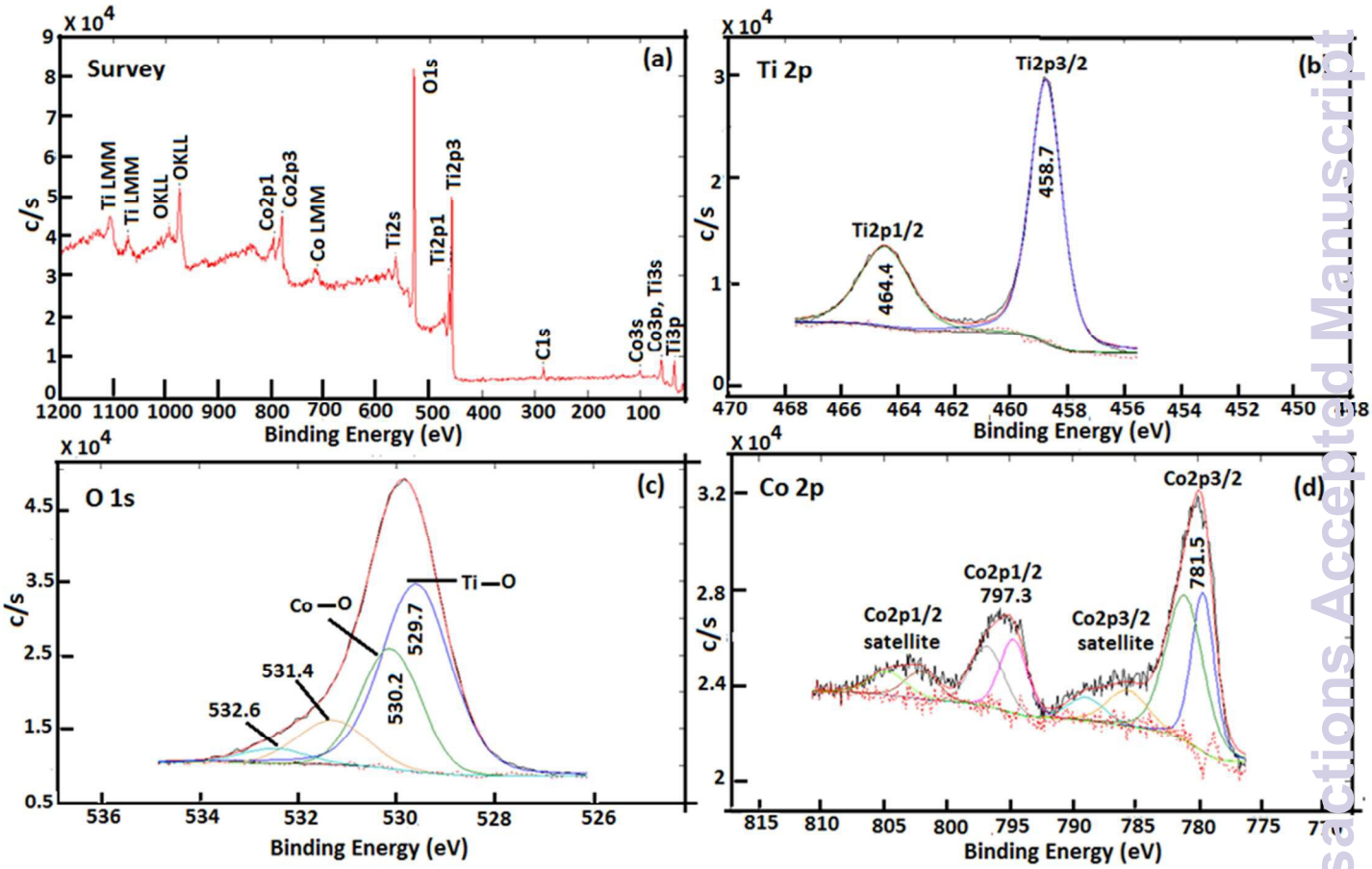

Figure 7: (**a**) XPS spectra of $CoTiO_3$-TiO_2 composite thin films prepared at 550 ˚C from ethanol solution of precursor (**1**) ; High resolution spectra $CoTiO_3$-TiO_2 for (**b**) Ti 2p (**c**) O 1s (**d**) Co 2p.

3.8 Electrochemical detection of dopamine (DA) by $CoTiO_3$-TiO_2 film electrode

3.8.1 CV behavior of DA

The $CoTiO_3$-TiO_2 composite film deposited at 550 ˚C was used for the electrocatalysis and sensing of dopamine (DA) in 0.1 M phosphate buffer solution (PBS) (pH 7.0). Fig. 8(**a**) represents cyclic voltammograms (CVs) both in absence and presence of DA in a phosphate

buffer solution, also containing 10 mM of Ascrobic acid (AA), a common interfering specie for DA.

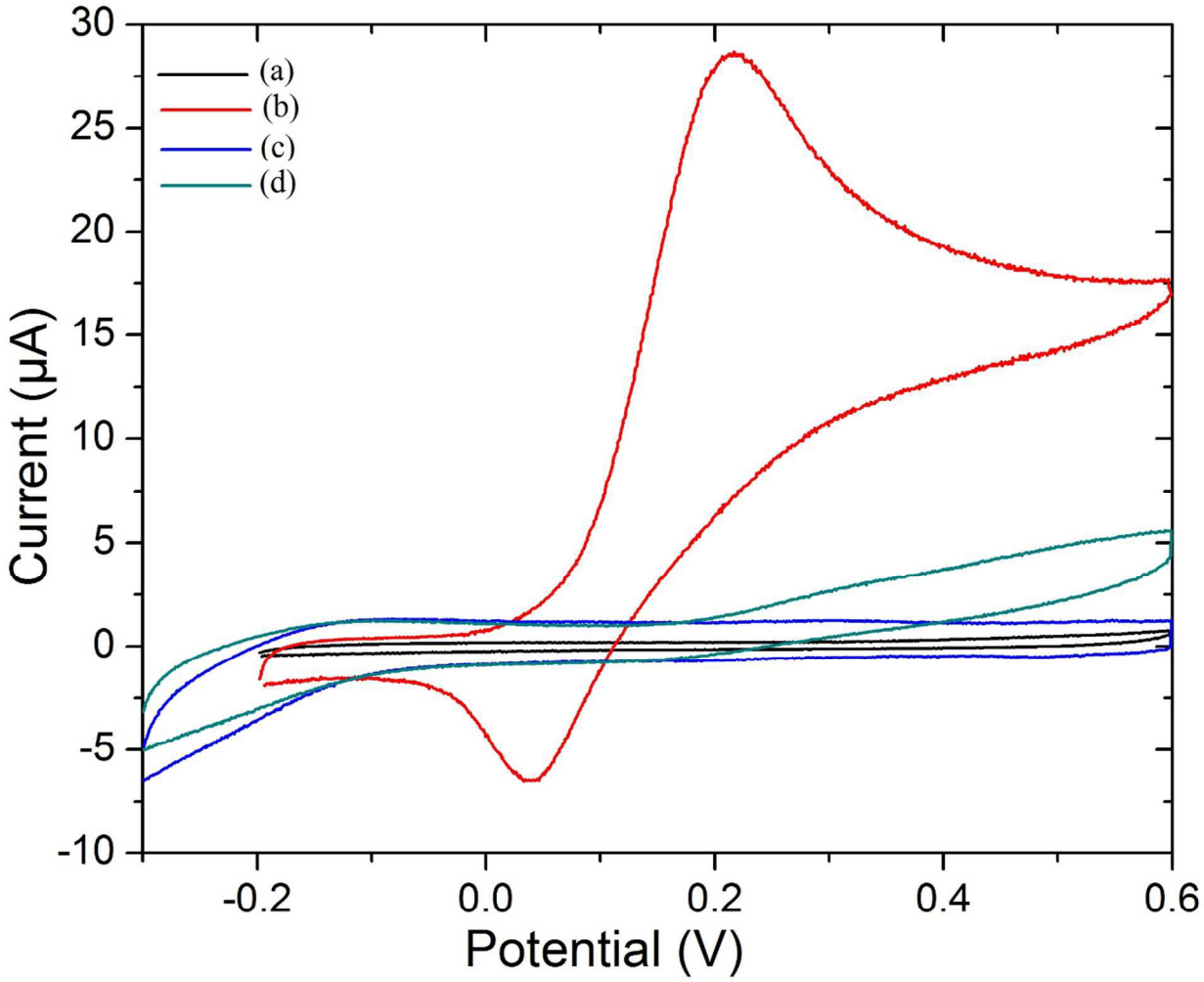

Figure 8: Cyclic voltammograms (**a**) absence, (**b**) presence of 15 μM DA obtained with the $CoTiO_3$-TiO_2 composite electrode; (**c**) absence and (d) presence of 50 μM DA recorded with the bare FTO electrode in the in 0.1 M PBS (pH 7.0) at a scan rate of 50 mV s^{-1}.

The potential was scanned between - 0.2 to + 0.6 V. It is evident from Fig. 8(**a**) that no redox peaks were observed in the absence of DA, which also infers that AA was not electrochemically active in this potential window. Fig. 8(**b**) represents that the $CoTiO_3$-TiO_2 composite electrode

displayed an intense and sharp anodic peak current at +0.215 V due to the electrocatalytic oxidation of dopamine when 15 μM of DA was present in the buffer solution. The corresponding reduction peak appeared at +0.075 V but with much less current density representing the quasi-reversible redox behavior of DA. The sharp peak for DA oxidation at +0.215 V was also indicative of fast electrode kinetics for the DA oxidation.[40,41]. To observe contribution from FTO towards DA oxidation, CVs in presence and absence of DA were recorded with bare FTO electrode as shown in figure 8c. The voltamograms indicate that in the absence of DA no redox peaks were observed and background current was higher than the $CoTiO_3$-TiO_2 composite electrode. In the presence of 50 μM of DA and AA, only a slight increase in current was observed with a broad oxidation peak starting from approximately 0.22 V and extending up to 0.6 V. These results clearly indicate that the $CoTiO_3$-TiO_2 composite electrode is capable to catalytically oxidize DA with a sharp oxidation peak within the tested potential window.

3.8.2 Effect of scan rate on CV studies

Further, influence of the potential scan rate on the electrocatalytic activity of DA at the $CoTiO_3$-TiO_2 film electrode surface was studied in the PBS (pH = 7.0) using CV, as shown in Fig. 9. increase in scan rate from 25 to 200mV/s led to the increase in both DA oxidation and reduction peaks with a slight shift in the peak potential. The shift in peak potential was due to the quasi-reversible redox process.[42] The linear relationship between the peak currents (I_p) and the square root of the scan rate was observed for both oxidation and reduction processes as shown in the inset of Fig.9. It is evident that, the anodic peak currents (I_{pa}) for the 10 μM DA varied linearly with the square root of the scan rate ($\nu^{1/2}$), with a linear regression equation, for anodic peak current I_{pa} (μA) = $0.0563\nu^{1/2}$ + 11.40 and a correlation coefficient R^2 = 0.985. This behavior suggests that the electrode kinetics is mainly diffusion controlled electrochemical reaction.

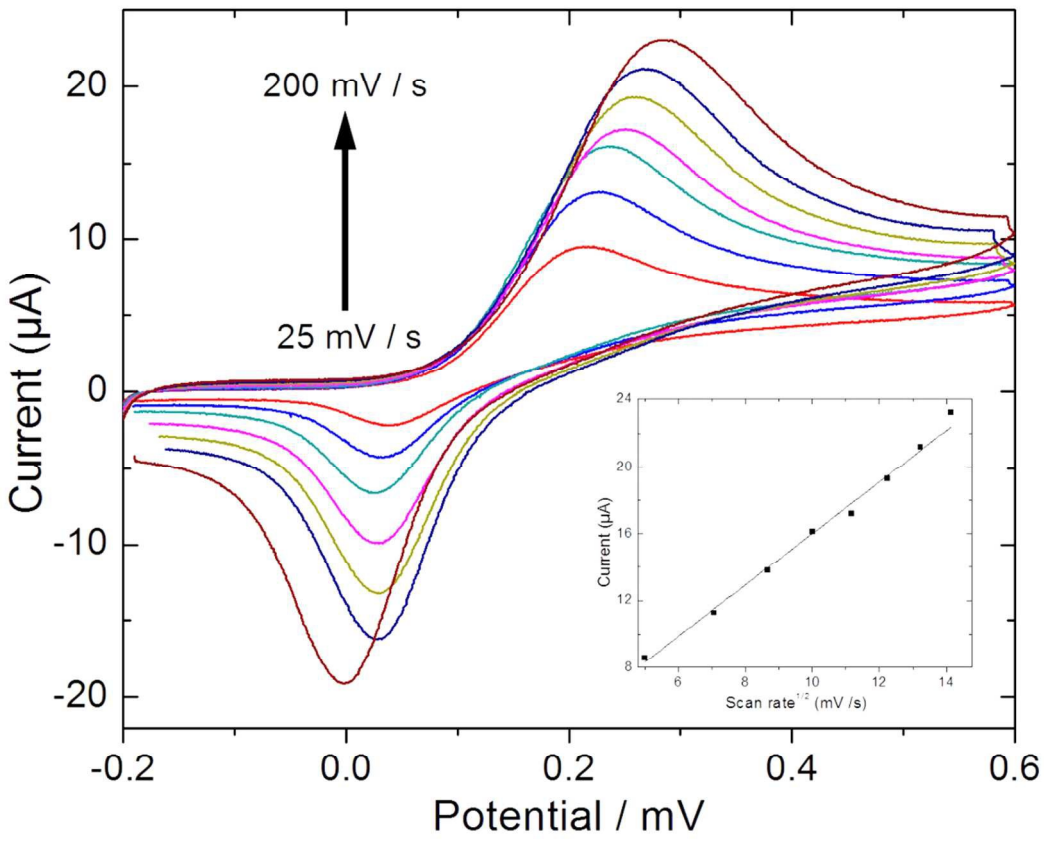

Figure 9: Cyclic voltammograms recorded for the $CoTiO_3$-TiO_2 electrode in the presence of 10 μM DA in 0.1 M PBS (pH 7.0) at various scan rates 25–200 mV s^{-1}. (Inset) Plot of anodic peak current vs. square root of the scan rate obtained with the $CoTiO_3$-TiO_2 electrode.

3.8.3 Effect of pH

pH plays a crucial role in the redox behaviour of DA at the $CoTiO_3$-TiO_2 film electrode surface. In fact, in CV experiments, redox couple of DA shifted towards the negative direction upon increasing the pH from 5-9, SI Fig.3. This infers that electrocatlaytic behaviour of DA is pH dependent. For practicality purposes, pH 7 was chosen for further analysis of DA with the $CoTiO_3$-TiO_2 composite electrode.

3.8.4 Analytical utilization

A series of linear scan voltammetry (LSV) curves were recorded in 0.1 M PBS (pH = 7.0) with different DA concentrations at the $CoTiO_3$-TiO_2 composite as shown in Fig. 10a. It could be observed that the anodic peak current increased linearly with an increase in the concentration of DA in the range of 20 to 300 µM, with $R^2 = 0.993$ (Fig. 10b). The sensitivity is determined from the slope of the calibration plot. The Fig. 10b shows the standard addition line with linear regression equation. The detection limit found was 0.083 µM (S/N = 6) by LSV. The sensitivity found from the slope was 0.325 µA. $\mu M^{-1}.cm^2$.

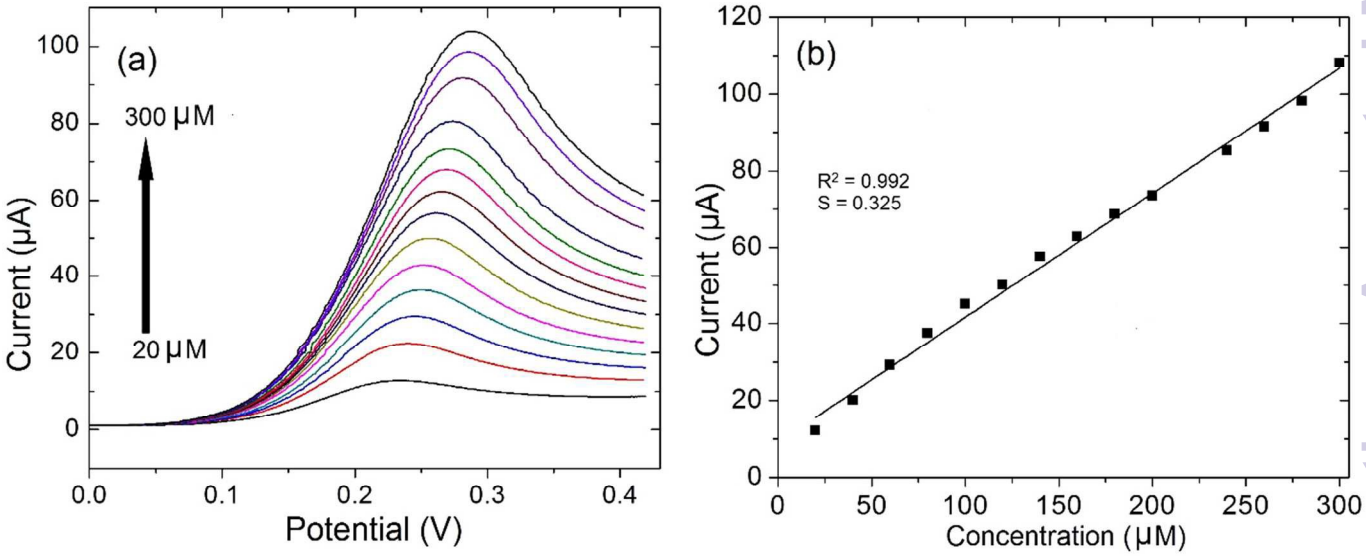

Figure 10: (a) LSV curves obtained with the $CoTiO_3$-TiO_2 composite electrode for various concentration of DA 0.1 M PBS (pH 7) at a scan rate of 50 mV s^{-1}. (b) Correlation between the concentration of DA and peak current for the $CoTiO_3$-TiO_2 electrode.

3.8.5 Selectivity and stability studies

The selectivity of the $CoTiO_3$-TiO_2 electrode towards DA oxidation was also investigated by LSV. Common interfering species AA, uric acid (UA), glucose, sulphate, nitrate and chloride were chosen and their effect on DA oxidation signal was evaluated as represented in Fig. 11. It is evident that even when 100-fold higher concentration of an interference source is used in a

homogeneously stirred of 0.1 M PBS (pH 7), there is no significant current response in the potential window used for DA analysis. This clearly suggested that DA oxidation at the fabricated $CoTiO_3$-TiO_2 composite was more selective and not affected in the presence of common interferences.

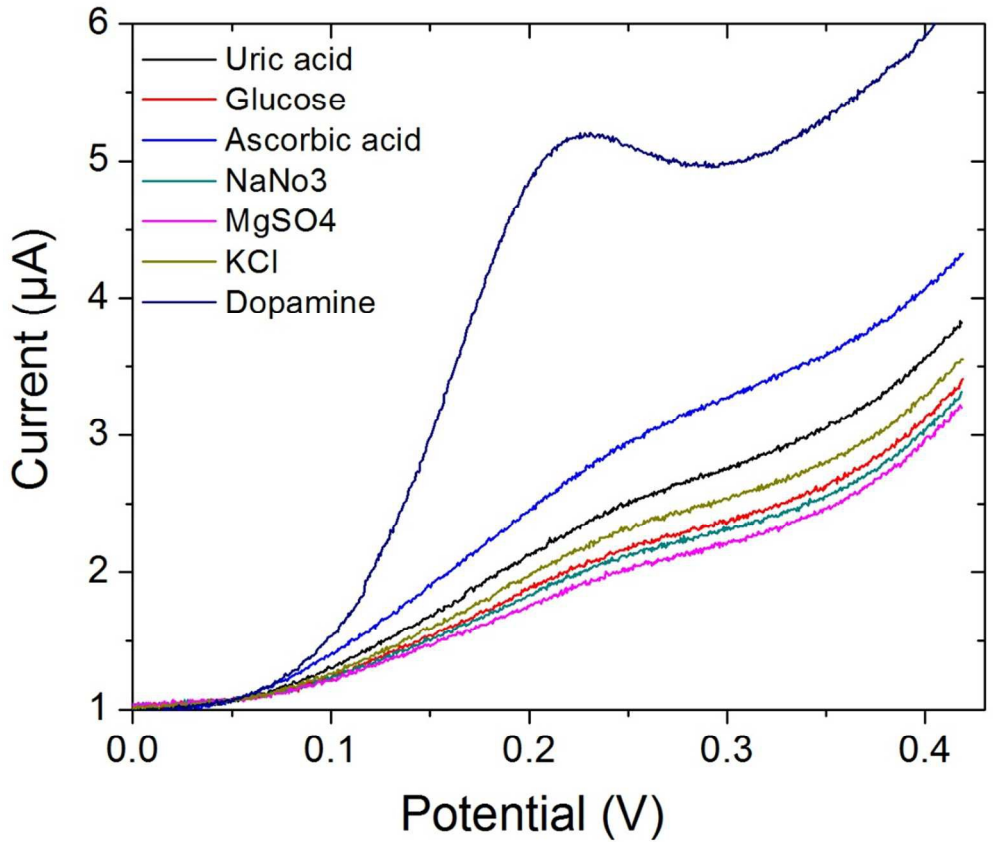

Figure 11: LSV response obtained with the $CoTiO_3$-TiO_2 composite electrode for 100 μM of each interferent and 10μM Dopamine in 0.1 M PBS (pH 7) at scan rate of 50 mV s^{-1}.

The stability of $CoTiO_3$-TiO_2 composite electrode was also monitored over the period of study. There was no significant loss observed in response for DA over 4 weeks with the standard deviation (RSD) of 3.4 %. Such a high stability of the $CoTiO_3$-TiO_2 composite electrode can be accredited to inherent properties of metal oxides compared to electrodes modified with pure metallic gold or platinium nanoparticles.[43]

The sensing performance of the $CoTiO_3$-TiO_2 film electrode was compared with other previously reported sensor materials for the detection of DA and the results are summarized in Table 2 which reveals that the present electrocatalyst performs equally good to the other bimetallic or metal oxide composite with carbon nanotubes (CNTs) and graphene oxide (GO) for the oxidation of DA.

It is very well known that the use of CNTs and GO provides large network for collecting electrons from oxidation process thereby assisting efficient current generation to improve the detection performance of electro catalyst. However, considering the prolong synthetic methods of these catalysts and high cost of Pt and Au metals, present catalyst prepared from AACVD technique is suitable alternative to Pt and Au free electrocatalyst for the DA oxidation with low cost and ease of fabrication.

Table 2: Comparison of analytical performance of various electrochemical sensors for DA detection

Sensor Material	**Analytical techniques**	**Limit of detection (LOD) (μM)**	**Ref.**
Au-Pt/GO-ERGO	Cyclic voltammetry	0.02	44
NiO–CuO/GR/GCE	Square Wave voltammetry	0.10	45
GO–La/CPE	Differential pulse voltammetry	0.00032	46
EPPGE-SWCNT–Fe_2O_3	Square Wave voltammetry	0.36	47
GO/SiO_2–MIPs/GCE	Amperometry	0.03	

			[48]
ZnO- GCE	Amperometry	0.06	[49]
Graphene–AuNPs	Differential pulse voltammetry	1.86	[43]
$CoTiO_3$-TiO_2	Linear scanning voltammetry	0.083	Present work

ERGO = Electrochemically reduced graphene oxide, GCE = glassy carbon electrode, CPE = Carbon paste electrode
GO = graphene oxide , MIP = molecularly imprinted polymers, EPPGE = edge-plane pyrolytic graphite electrode

4 Conclusions

The current work presents a synthetic route toward the design and synthesis of heterobimetallic compound, $[Co_2Ti_4(\mu\text{-}O)_6(TFA)_8(THF)_6]\cdot THF$ (**1**) by the interaction of cobalt (II) acetate tetrahydrate with titanium (IV) isopropoxide through a trifloroacetato bridging moeity in tetrahydofuran. The compound yields impurity free cobalttitanate-titania ($CoTiO_3$-TiO_2) composite oxide material on combustion at relatively low temperature of 500 ˚C. Henceforth, the complex (**1**) is appropriate for the deposition of $CoTiO_3$-TiO_2 composite oxide films on flourine doped tin oxide coated conducting substarte at different temperatures of 500, 550 and 600 ˚C via aerosol assisted chemical vapor deposition. Applicabilty of fabricated $CoTiO_3$-TiO_2 electrode in electrochemical sensor has been investigated towards the detection of dopamine (DA). The results indicate that $CoTiO_3$-TiO_2 electrode showed good electrocatalytic activity for DA with the limit of detection (LoD) of 0.083 μM and a linear range of 20 to 300 μM.

Supplementary data

CCDC 1453304 contains the supplementary crystallographic data for this paper. These data can be obtained free of charge from The Cambridge Crystallographic Data Centre via www.ccdc.cam.ac.uk/data_request/cif.

Electronic Supplementary Information (ESI) available: [Energy dispersive X-ray spectra]. See DOI: 10.1039/b000000x/

Acknowledgements

The authors acknowledge the High-Impact Research schemes grant numbers: UM.C/625/1/HIR/242, UMRG RP007-13AET and HIR-MOHE UM.S/P/628/3SC21 for funding.

References

1. I. Rossetti, *Current Inorganic Chemistry*, 2013, **3**, 50-69.
2. Y. J. Kim, B. Gao, S. Y. Han, M. H. Jung, A. K. Chakraborty, T. Ko, C. Lee and W. I. Lee, *The Journal of Physical Chemistry C*, 2009, **113**, 19179-19184.
3. Z. Jiao, T. Chen, J. Xiong, T. Wang, G. Lu, J. Ye and Y. Bi, *Scientific reports*, 2013, **3**.
4. S. Guo, J. Liu, S. Qiu, W. Liu, Y. Wang, N. Wu, J. Guo and Z. Guo, *Journal of Materials Chemistry A*, 2015, **3**, 23895-23904.
5. Y. Cai, Y. Ye, Z. Tian, J. Liu, Y. Liu and C. Liang, *Physical Chemistry Chemical Physics*, 2013, **15**, 20203-20209.
6. G. Krylova, A. Brioude, S. Ababou-Girard, J. Mrazek and L. Spanhel, *Physical Chemistry Chemical Physics*, 2010, **12**, 15101-15110.
7. S. E. Stanca, R. Müller, M. Urban, A. Csaki, F. Froehlich, C. Krafft, J. Popp and W. Fritzsche, *Catalysis Science & Technology*, 2012, **2**, 1472-1479.
8. T. Shukla, B. Yadav and P. Tandon, *Sensor Letters*, 2011, **9**, 533-540.
9. M. Siemons and U. Simon, *Sensors and Actuators B: Chemical*, 2007, **126**, 595-603.
10. M. Shilpy, M. A. Ehsan, T. H. Ali, S. B. A. Hamid and M. E. Ali, *RSC Advances*, 2015, **5**, 79644-79653.

11. P. Kapoor, S. Uma, S. Rodriguez and K. Klabunde, *Journal of Molecular Catalysis A: Chemical*, 2005, **229**, 145-150.
12. X. Zhang, B. Gao, L. Hu, L. Li, W. Jin, K. Huo and P. K. Chu, *CrystEngComm*, 2014, **16**, 10280-10285.
13. Y. Liang, Z. Cui, S. Zhu, Z. Li, X. Yang, Y. Chen and J. Ma, *Nanoscale*, 2013, **5**, 10916-10926.
14. P. Marchand and C. J. Carmalt, *Coordination Chemistry Reviews*, 2013, **257**, 3202-3221.
15. C. E. Knapp and C. J. Carmalt, *Chemical Society Reviews*, 2016.
16. P. Marchand, I. A. Hassan, I. P. Parkin and C. J. Carmalt, *Dalton Transactions*, 2013, **42**, 9406-9422.
17. M. A. Ehsan, H. N. Ming, V. McKee, T. A. N. Peiris, U. Wijayantha-Kahagala-Gamage, Z. Arifin and M. Mazhar, *New Journal of Chemistry*, 2014, **38**, 4083-4091.
18. M. A. Ehsan, A. A. Tahir, M. Hamid, M. Mazhar, K. U. Wijayantha and M. Zeller, *Inorganica Chimica Acta*, 2011, **376**, 189-194.
19. M. A. Ehsan, H. Khaledi, A. Pandikumar, N. M. Huang, Z. Arifin and M. Mazhar, *Journal of Solid State Chemistry*, 2015, **230**, 155-162.
20. M. A. Ehsan, H. Khaledi, A. Pandikumar, P. Rameshkumar, N. M. Huang, Z. Arifin and M. Mazhar, *New Journal of Chemistry*, 2015, **39**, 7442-7452.
21. M. A. Ehsan, H. Khaledi, Z. Arifin and M. Mazhar, *Polyhedron*, 2015, **98**, 190-195.
22. M. A. Ehsan, A. S. Hakeem, H. Khaledi, M. Mazhar, M. M. Shahid, A. Pandikumar and N. M. Huang, *RSC Advances*, 2015, **5**, 103852-103862.
23. M. A. Ehsan, M. A. Mansoor, M. Mazhar, A. A. Tahir, M. Hamid and K. Upul Wijayantha, *Applied Organometallic Chemistry*, 2012, **26**, 493.
24. Y. Deng, Q. Lv, S. Wu and S. Zhan, *Dalton Transactions*, 2010, **39**, 2497-2503.
25. Y.-F. Deng, H.-L. Zhang, Q.-M. Hong, W.-Z. Weng, H.-L. Wan and Z.-H. Zhou, *Journal of Solid State Chemistry*, 2007, **180**, 3152-3159.
26. Y.-F. Deng and Z.-H. Zhou, *Inorganic Chemistry Communications*, 2008, **11**, 1064-1066.
27. Y. Deng, S. Tang and S. Wu, *Solid State Sciences*, 2010, **12**, 339-344.
28. Y. Deng, S. Tang, Q. Zhang, Z. Shi, L. Zhang, S. Zhan and G. Chen, *Journal of Materials Chemistry*, 2011, **21**, 11987-11995.

29. S. A. Bakar, S. T. Hussain and M. Mazhar, *New Journal of Chemistry*, 2012, **36**, 1844-1851.
30. K. Jackowska and P. Krysinski, *Analytical and bioanalytical chemistry*, 2013, **405**, 3753-3771.
31. M. Hadi and A. Rouhollahi, *Analytica chimica acta*, 2012, **721**, 55-60.
32. G. M. Sheldrick, *Acta Crystallographica Section A: Foundations of Crystallography*, 2008, **64**, 112-122.
33. C. F. Macrae, P. R. Edgington, P. McCabe, E. Pidcock, G. P. Shields, R. Taylor, M. Towler and J. v. d. Streek, *Journal of applied crystallography*, 2006, **39**, 453-457.
34. R. Newnham, J. Fang and R. Santoro, *Acta Crystallographica*, 1964, **17**, 240-242.
35. P. Tomaszewski, *Wroclaw*, 2002, **1**, 1-123.
36. G. Zhou, D. K. Lee, Y. H. Kim, C. W. Kim and Y. S. Kang, *BULLETIN-KOREAN CHEMICAL SOCIETY*, 2006, **27**, 368.
37. S. H. Chuang, R. H. Gao, D. Y. Wang, H. P. Liu, L. M. Chen and M. Y. Chiang, *Journal of the Chinese Chemical Society*, 2010, **57**, 932-937.
38. F. Hardcastle, *J Ark Acad Sci*, 2011, **65**, 43-48.
39. N. T. Nolan, M. K. Seery and S. C. Pillai, *Chemistry of Materials*, 2011, **23**, 1496-1504.
40. J. Ping, J. Wu, Y. Wang and Y. Ying, *Biosensors and Bioelectronics*, 2012, **34**, 70-76.
41. L. Wu, L. Feng, J. Ren and X. Qu, *Biosensors and Bioelectronics*, 2012, **34**, 57-62.
42. D. Wu, H. Li, X. Xue, H. Fan, Q. Xin and Q. Wei, *Analytical Methods*, 2013, **5**, 1469-1473.
43. J. Li, J. Yang, Z. Yang, Y. Li, S. Yu, Q. Xu and X. Hu, *Analytical Methods*, 2012, **4**, 1725-1728.
44. Y. Liu, P. She, J. Gong, W. Wu, S. Xu, J. Li, K. Zhao and A. Deng, *Sensors and Actuators B: Chemical*, 2015, **221**, 1542-1553.
45. B. Liu, X. Ouyang, Y. Ding, L. Luo, D. Xu and Y. Ning, *Talanta*, 2016, **146**, 114-121.
46. F. Ye, C. Feng, N. Fu, H. Wu, J. Jiang and S. Han, *Applied Surface Science*, 2015, **357**, 1251-1259.
47. A. S. Adekunle, B. O. Agboola, J. Pillay and K. I. Ozoemena, *Sensors and Actuators B: Chemical*, 2010, **148**, 93-102.

48. Y. Zeng, Y. Zhou, L. Kong, T. Zhou and G. Shi, *Biosensors and Bioelectronics*, 2013, **45**, 25-33.

49. C. Xia, N. Wang, L. Wang and L. Guo, *Sensors and Actuators B: Chemical*, 2010, **147**, 629-634.

Graphical Abstarct

$CoTiO_3$-TiO_2 composite film electrode has been fabricated using single source precusor $[Co_2Ti_4(\mu\text{-}O)_6(TFA)_8(THF)_6]\cdot THF$ in aerosol assisted chemical vapour deposition and has been tested for electrochemical detection of dopamine.